Z. Phys. Chem. **223** (2009) 427–446 / **DOI** 10.1524/zpch.2009.6046

Formation of H-atoms in the Pyrolysis of 1,3-butadiene and 2-butyne: A Shock Tube and Modelling Study

By Sebastian Peukert, Clemens Naumann, and Marina Braun-Unkhoff*

DLR Institut für Verbrennungstechnik, Pfaffenwaldring 38–40, 70569 Stuttgart, Germany

Dedicated to Prof. Dr. Heinz-Georg Wagner on the occasion of his 80th birthday

(Received December 11, 2008; accepted March 8, 2009)

Shock Tube Technique / Chemical Kinetics / Surrogate Fuel / High Temperature Combustion / Reaction Mechanism

For investigating the pyrolysis of 1,3-butadiene (1,3-C_4H_6) and 2-butyne (2-C_4H_6), reactive gas mixtures highly diluted with argon as bath gas were prepared. The experiments were carried out in a high purity shock tube device over a temperature range of about 1500–1800 K at total pressures between 1.2 and 1.9 bar. The time-dependent formation of H-atoms was measured behind reflected shock waves by using the very sensitive method of atomic resonance absorption spectrometry (ARAS). A detailed chemical kinetic reaction mechanism consisting of 33 elementary reactions and 26 species was used to model the experimentally obtained H-atom profiles. From kinetic modelling, with help of sensitivity and reaction flux analysis, it was concluded that reaction R 1 2-C_4H_6 ↔ 2-C_4H_5 + H is crucial for the observed formation of H-atoms during the thermal decomposition of both investigated species and within the investigated range of temperatures and pressures. Moreover, at temperatures above about 1650 K, the decay of propargyl radicals (C_3H_3) turns out to contribute significantly to the amount of produced H-atoms. The following rate expressions were obtained for three reactions (R 1–R 3) – among them the isomerisation from 2-butyne to 1,3-butadiene – important with respect to the formation of H-atoms within the investigated parameter range. The uncertainties are estimated to be ±30%:

$$\text{2-}C_4H_6 \leftrightarrow \text{2-}C_4H_5 + H \qquad \text{(R 1)}$$

$$\text{2-}C_4H_6 \leftrightarrow \text{1,2-}C_4H_6 \qquad \text{(R 2)}$$

$$\text{1,3-}C_4H_6 \leftrightarrow C_2H_2 + C_2H_4 \qquad \text{(R 3)}$$

$$k_1 = 3.8 \cdot 10^{15} \exp(-44871\ K/T)\ \mathrm{s}^{-1}$$

$$k_2 = 6.9 \cdot 10^{13} \exp(-32496\ K/T)\ \mathrm{s}^{-1}$$

$$k_3 = 7.0 \cdot 10^{12} \exp(-33768\ K/T)\ \mathrm{s}^{-1}$$

* Corresponding author. E-mail: Marina.Braun-Unkhoff@dlr.de

1. Introduction

Practical fuels like diesel, gasoline, and kerosene may consist of blends of numerous species, among them many aliphatic, naphthenic, and aromatic compounds [1–4]. Consequently, the chemical kinetic modelling of their combustion behaviour is a challenging task, due to the complex composition. Using a detailed chemistry however, demands for an explicit knowledge of reaction kinetics and high computing power; hence, the complexity of chemical kinetic models must be reduced. For these reasons, to enable carrying out well defined experiments and simulating a combustion process, a surrogate or model fuel is introduced as a compromise to represent the practical fuel e.g. diesel or kerosene, with its numerous different species [5]. Surrogates include a limited number of hydrocarbons for which a kinetic reaction model must exist that is capable to describe characteristic combustion features such as ignition delay time, laminar flame speed, and eventually the formation of pollutants.

Moreover, model fuels are of high interest since they can be utilized to predict effects of chemical composition and fuel properties on the combustion process. As an example, nowadays, the numerical simulation of practical combustion processes occuring e.g. in gas turbines or engines is a well accepted tool for solving the problem of combustion control as well as to reduce emissions and fuel consumption. Consequently, to optimize new combustor designs it is necessary to couple experimental results with 3D-CFD calculations in order to shorten the time needed for development as well as their costs. To further promote the development of even more sophisticated combustion devices, a profound knowledge on the fuel combustion is inevitable. More over, to be predictive, a detailed chemical reaction mechanism is needed which is capable to describe the combustion of the investigated fuel correctly. Then, a validated reduced reaction model can be elaborated. Thus, the coupling of turbulence and detailed chemistry is possible.

In order to reproduce the kinetical properties of a complex fuel, one or two compounds from each chemical class (alkanes, cycloalkanes, alkenes, aromates) are selected in general to represent the individual chemical classes in a model fuel. For kerosene, as an example, cyclohexane (cyc-C_6H_{12}) or cyclohexene (cyc-C_6H_{10}) are mostly chosen to represent the (naphthenic) model fuel compound. Within this context, the formation of H-atoms must be described correctly, both in rate and amount, over the parameter range of interest, to be able to predict reliably main characteristic properties, in particular ignition behaviour and laminar flame speed.

The thermal decomposition of cyclohexene may take place via two initial reaction steps as a concurrence between C-H and C-C bondage split, respectively; the latter leading to the formation of 1,3-butadiene: cyc-$C_6H_{10} \leftrightarrow C_2H_4$ + 1,3-C_4H_6 [6–7].

Therefore, 1,3-butadiene is expected to be an important intermediate within the thermal decay of cyclohexene.

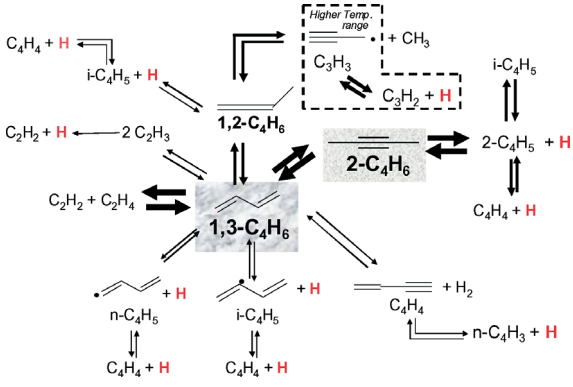

Fig. 1. Overview on reaction model describing pyrolysis system of 1,3 butadiene (1,3-C_4H_6) and 2-butyne (2-C_4H_6).

The pyrolysis of 1,3-butadiene has been studied previously by different methods [8–14]. However, no consistent picture exists, neither concerning the importance of the nature and the branching ratio of the initiation reactions nor the products formed.

For the reasons mentioned above, there is a need for a revisited analysis of the 1,3-butadiene system, also in the context of the thermal decay of cyclohexene. In the present work, two series of shock tube experiments on the pyrolysis of two C_4H_6-isomers, namely 1,3-butadiene (1,3-C_4H_6) and 2-butyne (2-C_4H_6) were carried out, at similar temperatures and pressures, by using very low initial reactant concentrations. The main purpose of the present work is to describe correctly the production of H-atoms in both combustion systems. A detailed reaction model comprising 33 reactions and 26 species was elaborated which is capable to match the measured H profiles over the whole investigated parameter range. Moreover, this reaction model allows also to predict experimental data of main species obtained by Laskin *et al.* [14] studying the pyrolysis of 1.3-butadiene in a plug flow reactor at atmospheric pressure.

2. Experimental

2.1 The shock tube apparatus

All experiments were performed in a stainless steel shock tube of 7.2 cm inner diameter separated by an aluminium diaphragm into a driver and driven section

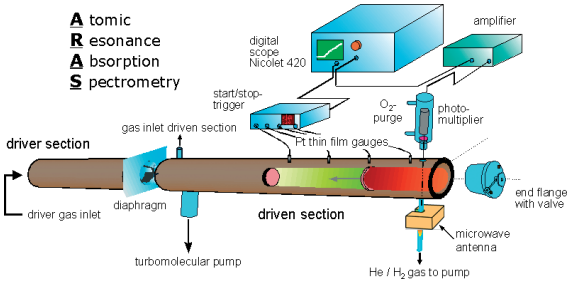

Fig. 2. Sketch of the experimental set-up.

of 4 m and 6.3 m in length, respectively. The apparatus is shown in Fig. 2, for details see ref. [19]. The shock waves were initiated by pressure bursting of the diaphragm using hydrogen as driver gas. The test gas in the low pressure part was argon of high purity with small quantities of 1,3-butadiene (2.0–6.0 ppm) or 2-butyne (2.0–6.0 ppm).

Reaction progress was monitored by the detection of H-atoms behind reflected shock waves in a measurement plane 10 mm away from the end plate of the tube. H-atom absorption was measured using ARAS at the Lyman α line (121.568 nm). For generating the vacuum-ultraviolet (VUV) radiation, a microwave discharge lamp was operated with 1% H_2 in He. The VUV radiation was transmitted through the shock tube via MgF_2-windows and collected by a solar blind photomultiplier (Thorn EMI / Electron Tubes 9403B). Spectral selectivity was achieved by a combination of a Lyman α interference filter (Acton Research, FWHM = 10 nm) together with an oxygen purge. The photomultiplier signal is intensified and bandwidth limited to 1 MHz by an amplifier (Stanford Research SR 560) and transmitted to a storage oscilloscope (Nicolet 410). The experimental observation period was 800 μs. The storage oscilloscope is triggered by the last thin film gauge before the end plate of the tube.

The velocity of the incident shock wave was measured by four thin film platinum gauges. Thus, with the known initial temperature and pressure of the test gas, the state variables of the shock heated test gas mixture (temperature, pressure, density) behind the reflected shock wave was calculated solving the Rankine-Hugoniot equations and applying the ideal gas law [20].

The test gas mixtures were prepared in a stainless steel vessel heated to a temperature of 393 K. Before filling, it was evacuated to pressures below $1 \cdot 10^{-6}$ mbar. After preparation of a new test gas mixture, the gas mixture was allowed to homogenise for at least 4 h prior to use. The initial concentrations of the reactants as well as their purity were checked by gas chromatographic analysis (GC-FID).

The purity of the used gases and chemicals were as follows: 1,3-butadiene (Linde) ~ 99.0%, 2-butyne (Sigma-Aldrich) ~ 99.0%, Ar as inert gas (Linde) ~ 99.9999%, H_2 (Linde) as driver gas > 99.8%. For the calibration of H-ARAS a

gas mixture (AGA Gas GmbH) was used containing N_2O (2.0±0.10 ppm), H_2 (207±10 ppm), rest Ar.

The advantage of working with very low initial species concentrations being typical for ARAS studies generally need measures to exclude a possible influence of any sources that might contribute to the observable under consideration, e.g. H-atoms.

Impurities either present in the reactive mixture or in the reactor's gas phase have to be avoided. Moreover, compounds adsorbed onto the shock tube walls may desorb into the gas phase and thus, even in extremely low quantities, might influence the reaction process. For this reason, the shock tube was evacuated by a turbo molecular pump down to pressures lower than $1 \cdot 10^{-6}$ mbar and permanently heated to 373 K. Furthermore, before each series of measurements, the degree of cleanliness of the shock tube was checked by measuring H-atom background absorption at Lyman α at temperatures above 2200 K. In our experiments, this background absorption was always below 5% corresponding to a H-atom concentration of ~ $3 \cdot 10^{11}$ cm^{-3}. Thus, we can rule out effects of background absorption on the measured H absorption profiles.

2.2 The calibration procedure

As mentioned above, the formation of H-atoms was monitored by ARAS at the Lyman α line. The light source is a microwave generated plasma discharge fed by a 1% H_2 in helium gas mixture. The limit of H-atom concentration corresponds to ~ $3 \cdot 10^{11}$ cm^{-3}. Due to the high sensitivity of this method, highly diluted reaction gas mixtures can be used for experimental investigations. This enables studying elementary reaction kinetics with only minor influence of subsequent reactions.

Unfortunately, the correlation between measured absorption and absorber concentration is complicated by the self-reversal of the emission profile at the resonance frequency [21]. Decreasing Doppler broadening of the H-atoms due to temperature gradients along the optical axis of the discharge lamp leads to a resonant absorption of the central line by "cooler" H-atoms whereas the emitted light from the "spectral wings" of the hottest zone can escape. Because of this complex spectral profile, calibration of the detection system becomes indispensable. Therefore, we use the well-established reaction sequence starting with N_2O (+ M) → N_2 + O (+ M) via H_2 + O → OH + H and OH + H_2 → H_2O + H to produce H-atoms initialising the reaction system with known concentrations of N_2O and H_2 diluted in Ar [22–23]. Below temperatures of about 2000 K, a quasi-stationary concentration profile of H-atoms cannot be achieved within the observation period. Thus, measurements below this temperature use the dynamical increase of the absorption to link it to the respective absorber concentration. Above 2000 K, a constant absorption level is reached until H_2-dissociation starts.

The functional relationship between absorber concentration and absorption can be fitted to a modified Lambert-Beer equation:

$$A = 1 - \exp(l \cdot [X]^n \cdot s^{3n-1}) \quad (1)$$

with A: absorption; l: absorption path length in cm; $[X]$: concentration of absorber in cm^{-3}; for $n = 1$, s^2 corresponds to the classical absorption cross section σ, whereas n is an additional fitting parameter providing a better correlation to X = X(A). Within the temperature range of this investigation, no temperature dependence on the calibration was found.

3. Results and discussion

In the present work, a comprehensive study was done on the pyrolysis system of two C_4H_6-iosmers, at combustion relevant temperatures and at elevated pressures. In particular, the rate and the amount of H-atoms formed within the overall combustion process was intended to be described correctly by a detailed reaction model.

For this purpose, two series of H-ARAS (Atomic Resonance Absorption Spectrometry) shock tube experiments were carried out investigating the thermal decomposition of two C_4H_6-isomers, namely 1,3-butadiene (1,3-C_4H_6) and 2-butyne (2-C_4H_6). Both series were run at similar temperatures and pressures, using very low initial concentrations, to minimize the influence of secondary reactions. The main goal of the present work is to describe correctly the production of H-atoms in *both* reaction systems, by using the *same* reaction model.

It will be shown that the detailed reaction model comprising 33 reactions and 26 species elaborated within the present work (see Table 1) is capable to match the measured H-profiles over the whole investigated parameter range. Moreover, this reaction model allows also to predict experimental data of major species measured by Laskin *et al.* in a plug flow reactor experiment studying the decomposition of 1,3-butadiene, at atmospheric pressure and temperatures around 1200 K [14] (see Fig. (11)).

3.1 Modelling procedure and thermodynamics

Typical experimental H-atom-profiles are displayed in Fig. 3, for both investigated reactants, normalized to the initial concentration of the reactant. According to this figure, the thermal decomposition of 2-C_4H_6 yields a larger amount of H-atoms compared to the one of 1,3-butadiene, for similar conditions (temperature, pressure, initial concentration).

For modelling the measured H-atom absorption time profiles, an adaptation of the SENKIN code of the CHEMKIN II programme suite was used [25]. If not otherwise stated, the rate of each elementary reaction was computed for both directions; those of the reverse reaction were obtained from the k-values of the forward reaction and the equilibrium constant. If available, the thermodynamic properties of the species (see Table 2) were mostly taken from reference [26], otherwise from [27].

Table 1. Reaction model for the decomposition of 1,3-butadiene and 2-butyne. Reaction coefficient $k = A\ T^n \exp(-E_a/RT)$; units cm, s, mol, cal. Values for E_a are given in cal·mol^{-1}.

No.	Reaction		A	n	E_a	Reference
R 1	$2\text{-}C_4H_6 \leftrightarrow 2\text{-}C_4H_5 + H$		$3.8 \cdot 10^{15}$	0.0	89200.0	This work
R 2	$2\text{-}C_4H_6 \leftrightarrow 1,2\text{-}C_4H_6$		$6.9 \cdot 10^{13}$	0.0	64600.0	This work
R 3	$1,3\text{-}C_4H_6 \leftrightarrow C_2H_2 + C_2H_4$		$7.0 \cdot 10^{12}$	0.0	67100.0	This work
R 4	$2\text{-}C_4H_6 \leftrightarrow 1,3\text{-}C_4H_6$		$3.0 \cdot 10^{13}$	0.0	65000.0	[15]
R 5	$1,2\text{-}C_4H_6 \leftrightarrow 1,3\text{-}C_4H_6$		$2.5 \cdot 10^{13}$	0.0	63000.0	[15]
R-6	$C_2H_3 + C_2H_3 \leftrightarrow 1,3\text{-}C_4H_6$		$1.5 \cdot 10^{42}$	−8.8	12483.0	[29]
R 7	C_2H_3 (+M) $\leftrightarrow C_2H_2 + H$ (+M)					[30]
		k_∞	$3.9 \cdot 10^{8}$	1.62	37048.2	
		k_0	$2.6 \cdot 10^{27}$	−3.40	35798.7	
	TROE a = 1.982 ; T^{***} = 5383.7		T^{*} = 4.3			
R 8	$1,3\text{-}C_4H_6 \leftrightarrow C_4H_4 + H_2$		$2.5 \cdot 10^{15}$	0.0	94700.0	[15]
R 9	$1,3\text{-}C_4H_6 \leftrightarrow i\text{-}C_4H_5 + H$		$5.7 \cdot 10^{36}$	−6.3	112353.0	[29]
R 10	$1,3\text{-}C_4H_6 \leftrightarrow n\text{-}C_4H_5 + H$		$5.3 \cdot 10^{44}$	−8.6	123608.0	[29]
R 11	$C_3H_3 + CH_3$ (+M) $\leftrightarrow 1,2\text{-}C_4H_6$ (+M)					[29]
		k_∞	$1.5 \cdot 10^{12}$	0.0	0.0	
		k_0	$2.6 \cdot 10^{57}$	−11.9	9770.0	
	TROE a = 0.175 T^{***} = 1340.6		T^{*} = 60000.0	T^{**} = 9769.8		
R 12	$C_3H_3 \leftrightarrow C_3H_2 + H$		$7.65 \cdot 10^{12}$	0.0	78365.0	[32]
R 13	$C_3H_3 + C_3H_3 \leftrightarrow$ phenyl + H		$3.0 \cdot 10^{11}$	0.0	0.0	[32]
R 14	$C_3H_3 + C_3H_3 \leftrightarrow$ benzene		$6.5 \cdot 10^{12}$	0.0	0.0	[32]
R 15	$1\text{-}C_4H_6 \leftrightarrow 1,2\text{-}C_4H_6$		$2.5 \cdot 10^{13}$	0.0	65000.0	[16]
R 16	$1\text{-}C_4H_6 \leftrightarrow C_3H_3 + CH_3$		$3.0 \cdot 10^{15}$	0.0	75800.0	[16]
R 17	$1,2\text{-}C_4H_6 \leftrightarrow i\text{-}C_4H_5 + H$		$4.2 \cdot 10^{15}$	0.0	92600.0	[31]
R 18	$2\text{-}C_4H_5 \leftrightarrow i\text{-}C_4H_5$		$5.0 \cdot 10^{12}$	0.0	50500.0	[33]
R 19	$2\text{-}C_4H_5 \leftrightarrow t\text{-}C_4H_4 + H$		$6.0 \cdot 10^{13}$	0.0	53000.0	[33]
R 20	$t\text{-}C_4H_4 + H \leftrightarrow H_2 + i\text{-}C_4H_3$		$3.0 \cdot 10^{7}$	2.0	6000.0	[33]
R 21	$C_2H_4 + Ar \leftrightarrow C_2H_3 + H + Ar$		$2.6 \cdot 10^{17}$	0.0	96512.0	[34]
R 22	$CH_3 + Ar \leftrightarrow CH + H_2 + Ar$		$3.1 \cdot 10^{15}$	0.0	80836.0	[35]
R 23	$CH_3 + Ar \leftrightarrow CH_2 + H + Ar$		$2.2 \cdot 10^{15}$	0.0	82624.0	[35]
R 24	$CH_3 + CH_3 \leftrightarrow C_2H_5 + H$		$3.0 \cdot 10^{13}$	0.0	13506.0	[36]
R 25	$C_2H_5 \leftrightarrow C_2H_4 + H$		$8.2 \cdot 10^{12}$	0.0	39895.0	[34]
R 26	$C_4H_4 \leftrightarrow C_2H_2 + C_2H_2$		$3.4 \cdot 10^{13}$	0.0	77102.0	[37]
R 27	$C_4H_4 \leftrightarrow C_4H_2 + H_2$		$1.3 \cdot 10^{15}$	0.0	94680.0	[37]
R 28	$C_4H_4 + Ar \leftrightarrow n\text{-}C_4H_3 + H + Ar$		$1.1 \cdot 10^{20}$	0.0	99109.0	[37]
R 29	$C_4H_2 + H \leftrightarrow n\text{-}C_4H_3$		$1.1 \cdot 10^{42}$	−8.7	15300.0	[29]
R 30	$C_4H_4 + H \leftrightarrow n\text{-}C_4H_5$		$1.3 \cdot 10^{51}$	−11.9	16500.0	[29]
R 31	$C_4H_4 + H \leftrightarrow i\text{-}C_4H_5$		$4.9 \cdot 10^{51}$	−11.9	17700.0	[29]
R 32	$n\text{-}C_4H_3 + H \leftrightarrow C_4H_4$		$2.0 \cdot 10^{47}$	−10.3	13070.0	[38]
R 33	$i\text{-}C_4H_3 + H \leftrightarrow C_4H_4$		$3.4 \cdot 10^{43}$	−9.0	12120.0	[38]

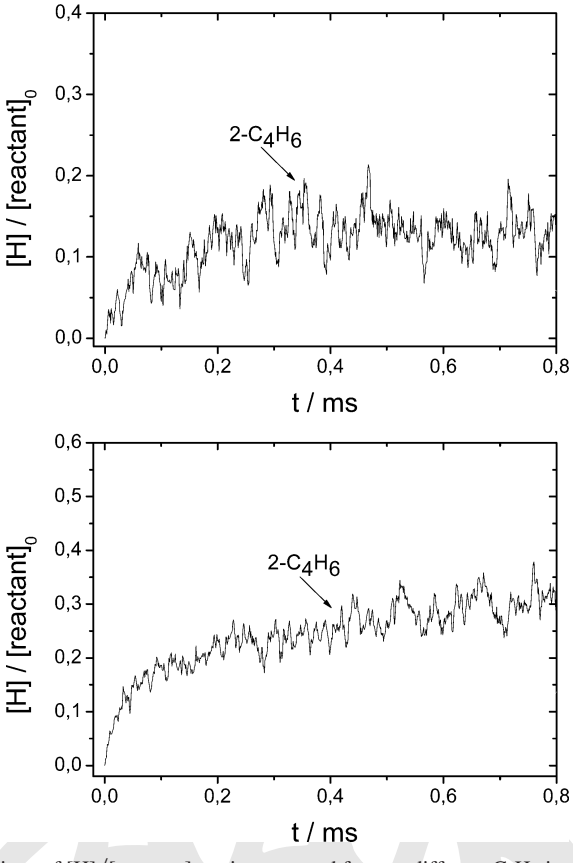

Fig. 3. Comparison of [H]/[reactant]$_0$-ratio measured for two different C_4H_6-isomers. Top: T_5 = 1603 K, p_5 = 1.91 bar, Bottom: T_5 = 1685 K, p_5 = 1.93 bar.

3.2 Comparison with results of former investigations

The thermal decomposition of 1,3-butadiene may take place via different initial reaction steps, as a competition between C-H and C-C bondage split. Presently, no comprehensive understanding about the branching ratio and the reaction rate expressions of the several initiation steps of 1,3-butadiene reaction system exists. This may be attributed to the existence of further C_4H_6-isomers, with 2-butyne and 1,2-butadiene among them.

$$2\text{-}C_4H_6 \leftrightarrow 1,3\text{-}C_4H_6 \quad \text{(R 4)}$$

$$1,2\text{-}C_4H_6 \leftrightarrow 1,3\text{-}C_4H_6 \quad \text{(R 5)}$$

Kiefer *et al.* [10, 11] proposed the decomposition of 1,3-butadiene yielding two vinyl radicals (C_2H_3) as being the primary reaction step, followed by a fast decay into acetylene + H:

Table 2. Heat of formation values of important species used in the present work, mostly taken from Wang [26]. Values are given in *kcal mol*$^{-1}$.

Species	$\Delta H^0_{f,\,298}$
1,3-C_4H_6 (1,3-butadiene)	26.3
1,2-C_4H_6 (1,2-butadiene)	39.3
2-C_4H_6 (2-butyne)	34.7
1-C_4H_6 (1-butyne)	39.5 [27]
C_4H_4 (vinyl acetylene)	68.0
C_2H_2 (acetylene)	54.5
C_2H_4 (ethylene)	12.6
n-C_4H_5 (2-butene-1-yl)	85.4
i-C_4H_5 (2-butene-2-yl)	77.4
C_3H_3 (propargyl radical)	82.7
CH_3 (methyl radical)	35.1
C_2H_3 (vinyl radical)	71.6

$$1,3\text{-}C_4H_6 \leftrightarrow C_2H_3 + C_2H_3 \qquad \text{(R 6)}$$

$$C_2H_3\ (+M) \leftrightarrow C_2H_2 + H + (M) \qquad \text{(R 7)}$$

On the other side, Skinner and Sokolowski [8] and Hidaka *et al.* [15] found from their single pulse shock tube experiments an approximate ratio of 1:1 of the reaction products acetylene (C_2H_2) and ethylene (C_2H_4), which can not be explained by the findings of Kiefer *et al.* [10, 11]. Furthermore, H-ARAS shock tube experiments carried out by Skinner and co-workers on the pyrolysis of 1,3-butadiene [12] support the conclusion of (R 6) being relatively unimportant.

A new aspect for understanding the thermal decomposition of 1,3-butadiene was added by Hidaka *et al.* [15]. They pointed out that the isomerisation reactions between the four butadiene isomers play an important role within the C_4H_6-decomposition system. Therefore, they carried out further shock tube studies investigating the pyrolysis of 1,2-butadiene (1,2-C_4H_6) [16] and 2-butyne (2-C_4H_6) [17]. Based on these studies, combined experimental and theoretical mechanistic studies on the procedures of isomerisation reactions were published [18].

Finally, Laskin *et al.* [14] investigated the 1,3-butadiene pyrolysis within a temperature range of 1100 and 1200 K at atmospheric pressure in a plug flow reactor experiment and developed a reaction mechanism capable to reproduce their measured stable species profiles.

Using the detailed chemical kinetic reaction model elaborated in the present work (see Table 1), H-atom profiles obtained within the pyrolysis of 1,3-butadi-

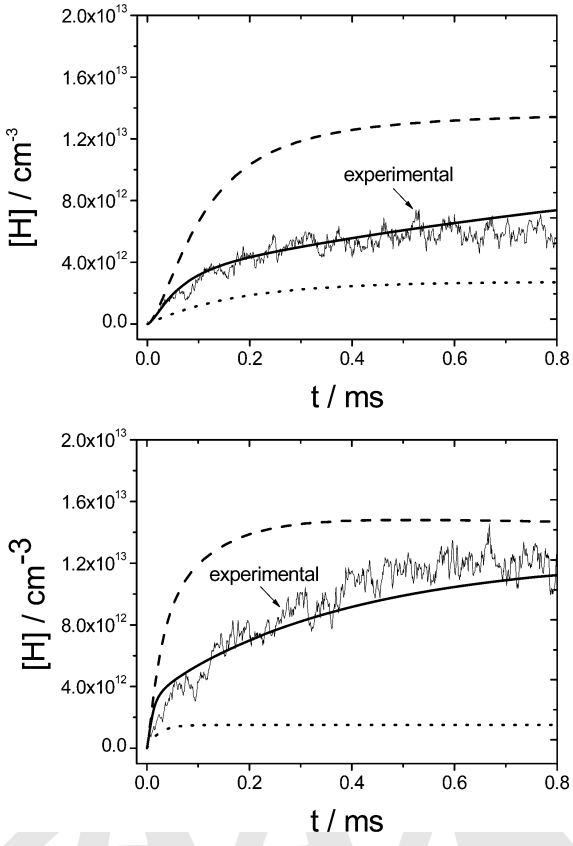

Fig. 4. Comparison between measured and computed H-atom profiles using different reaction models. Solid curve: reaction model, present work; dashed curve: reaction model, Laskin *et al.* [14]; dotted curve: reaction model, Rao *et al.* [12]. Top: T_5 = 1661 K, p_5 = 1.78 bar, $[1,3\text{-}C_4H_6]_0$ = 5.4 ppm diluted with argon. Bottom: T_5 = 1805 K, p_5 = 1.92 bar, $[1,3\text{-}C_4H_6]_0$ = 3.0 ppm diluted with argon.

ene and 2-butyne, respectively, were reproduced (see Fig. 4, solid curves). On the other hand, the reaction model published by Laskin *et al.* [14] under predicts the measured H-atom profile (Fig. 4, dotted curves), whereas the one given by Rao *et al.* [12] over predicts the measured H-atom profiles, in particular for the early stage of the investigated time interval (Fig. 4, dashed curve).

3.3 Perturbation sensitivity analysis

Perturbation sensitivity analysis was carried out for both educts, 1,3-butadiene (see Figs. 5a–6a) and 2-butyne (see Figs. 6b–7b), for the same initial conditions (i) in order to identify the reaction steps having a significant impact on the time

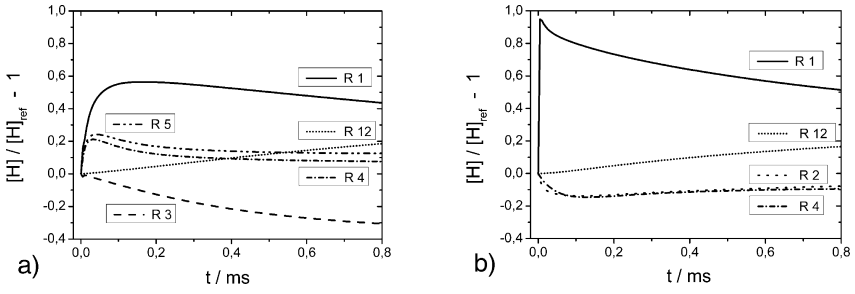

Fig. 5. a) Perturbation sensitivity plot, for 1,3-butadiene: T_5 = 1530 K, p_5 = 1.86 bar, [1,3-C_4H_6]$_0$ = 3.8 ppm, diluted with argon. R1: 2-C_4H_6 ↔ 2-C_4H_5 + H; R3: 1,3-C_4H_6 ↔ C_2H_4 + C_2H_2; R4: 2-C_4H_6 ↔ 1,3-C_4H_6; R5: 1,2-C_4H_6 ↔ 1,3-C_4H_6; R12: C_3H_3 ↔ C_3H_2 + H. b) Perturbation sensitivity plot for 2-butyne: T_5 = 1530 K, p_5 = 1.86 bar, [2-C_4H_6]$_0$ = 3.8 ppm, diluted with argon. R1: 2-C_4H_6 ↔ 2-C_4H_5 + H; R2: 2-C_4H_6 ↔ 1,2-C_4H_6; R4: 2-C_4H_6 ↔ 1,3-C_4H_6; R12: C_3H_3 ↔ C_3H_2 + H.

dependent progress of H-atom formation and (ii) to find out if main differences between those two combustion systems exist. This procedure was followed by the kinetic modelling of the most sensitive reactions. For this analysis procedure, the developed detailed reaction model comprising 33 elementary reactions was used (see Table 1) which matches the H-atom concentration profiles obtained during the thermal decomposition of *both* educts, 1,3-butadiene *and* 2-butyne.

By varying the rate coefficient values for each reaction, a perturbation sensitivity analysis was carried out for different experimental conditions covering in particular the temperature range of the experiments and yielding the variances in concentration time progress for H-atoms. The H-concentration time-profiles, simulated under the condition that no rate coefficient value is changed (*i. e.* multiplication with 1), are referred to as reference profiles $[X]_{ref}(t)$. The deviant profiles are obtained if the rate coefficient values for the forward and reverse direction of a reaction are multiplied with a certain factor f referred to $f = n$ as $[X]_{f=n}(t)$. The deviation δ from the reference is then given by:

$$\delta = \frac{[X]_{f=n}(t)}{[X]_{ref}(t)} - 1 \qquad (2)$$

with: [X]: concentration of the investigated species, *i.e.* [H].

In the present study, the rate coefficient values for each reaction were changed by multiplication by a factor $f = 2$. In Figs. 5–6, the deviations according to (Eq. 2) were plotted as a function of reaction time for both reactants: 1,3-butadiene (Figs. 5a–6a) and 2-butyne (Figs. 5b–6b). Two different experimental conditions were selected as typical for the lower and upper range of the investigated temperature range of the experiments conducted in the present work. For clarity, the deviations are shown only for reactions with a value of $\delta > 0.1$.

Concerning the pyrolysis of 1,3-butadiene, Figures 5a–6a show that mainly four reactions (R 1, R3–R5) have a considerable impact on the time dependency

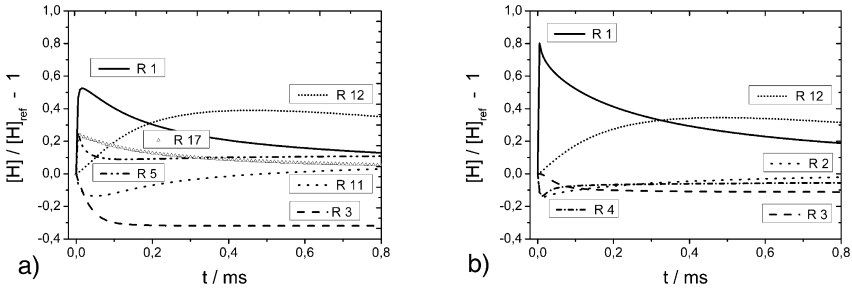

Fig. 6. a) Perturbation sensitivity plot, for 1,3-butadiene: T_5 = 1715 K, p_5 = 1.84 bar, [1,3-$C_4H_6]_0$ = 2.9 ppm, diluted with argon. R1: 2-C_4H_6 ↔ 2-C_4H_5 + H, R3: 1,3-C_4H_6 ↔ C_2H_4 + C_2H_2; R5: 1,2-C_4H_6 ↔ 1,3-C_4H_6; R11: C_3H_3 + CH_3 (+M) ↔ 1,2-C_4H_6 (+M); R12: C_3H_3 ↔ C_3H_2 + H; R17: 1,2-C_4H_6 ↔ i-C_4H_5 + H. b) Perturbation sensitivity plot, for 2-butyne: T_5 = 1715 K, p_5 = 1.84 bar, [2-$C_4H_6]_0$ = 2.9 ppm, diluted with argon. R1: 2-C_4H_6 ↔ 2-C_4H_5 + H; R2: 2-C_4H_6 ↔ 1,2-C_4H_6; R3: 1,3-C_4H_6 ↔ C_2H_4 + C_2H_2; R4: 2-C_4H_6 ↔ 1,3-C_4H_6; R12: C_3H_3 ↔ C_3H_2 + H.

of the H-formation, at the lower end of the investigated temperature range (1520–1700 K):

$$2\text{-}C_4H_6 \leftrightarrow 2\text{-}C_4H_5 + H \qquad (R\ 1)$$
$$1,3\text{-}C_4H_6 \leftrightarrow C_2H_4 + C_2H_2 \qquad (R\ 3)$$
$$2\text{-}C_4H_6 \leftrightarrow 1,3\text{-}C_4H_6 \qquad (R\ 4)$$
$$1,2\text{-}C_4H_6 \leftrightarrow 1,3\text{-}C_4H_6 \qquad (R\ 5)$$

For higher temperatures, (1700 < T < 1920 K) further reactions were identified as important:

$$C_3H_3 + CH_3\ (+M) \leftrightarrow 1,2\text{-}C_4H_6\ (+M) \qquad (R\ 11)$$
$$C_3H_3 \leftrightarrow C_3H_2 + H \qquad (R\ 12)$$
$$1,2\text{-}C_4H_6 \leftrightarrow i\text{-}C_4H_5 + H \qquad (R\ 17)$$

Concerning the pyrolysis of 2-butyne, Figures 5b–6b show that mainly four reactions (R 1, R 2, R4, and R 12) are sensitive to the H-atom concentration profile. They have a considerable impact on the time dependence of the H-formation, at the lower end of the investigated temperature range (1520–1700 K); whereas for higher temperatures the decay of propargyl radicals yielding H-atoms via (R 12) has to be considered also:

$$2\text{-}C_4H_6 \leftrightarrow 2\text{-}C_4H_5 + H \qquad (R\ 1)$$
$$2\text{-}C_4H_6 \leftrightarrow 1,2\text{-}C_4H_6 \qquad (R\ 2)$$
$$1,3\text{-}C_4H_6 \leftrightarrow C_2H_4 + C_2H_2 \qquad (R\ 3)$$
$$2\text{-}C_4H_6 \leftrightarrow 1,3\text{-}C_4H_6 \qquad (R\ 4)$$
$$C_3H_3 \leftrightarrow C_3H_2 + H \qquad (R\ 12)$$

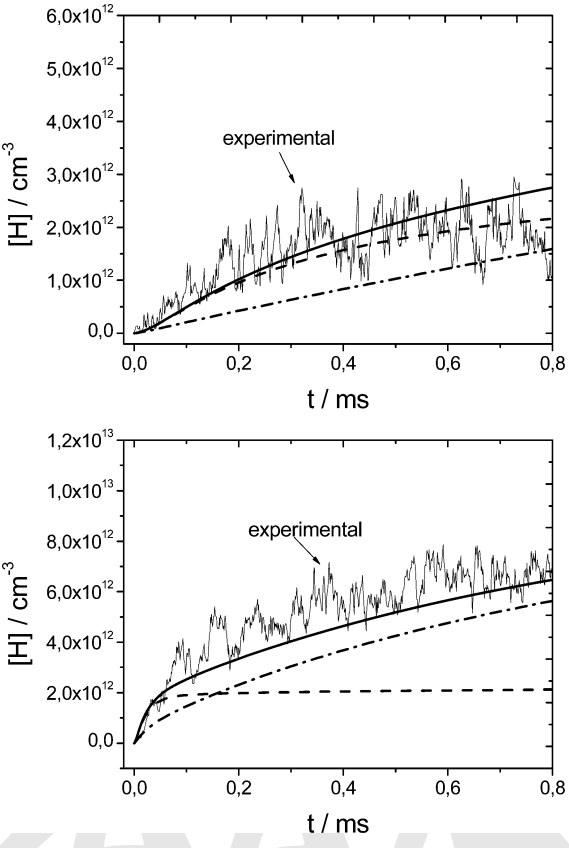

Fig. 7. Influence of reactions (R 1) and (R 12) on H-atom production. Solid curve: full mechanism; dashed curve: without (R 12); dash-dotted curve: without (R 1). Top: T_5 = 1547 K, p_5 = 1.94 bar, $[1,3\text{-}C_4H_6]_0$ = 6.0 ppm, diluted with argon. Bottom: T_5 = 1736 K, p_5 = 1.82 bar, $[1,3\text{-}C_4H_6]_0$ = 2.7 ppm, diluted with argon.

3.4 Kinetic modelling

Concerning the thermal decomposition of *both* investigated isomeres, reaction (R 1) $2\text{-}C_4H_6 \leftrightarrow 2\text{-}C_4H_5 + H$ is comparatively important for the production of H-atoms over the whole range of temperatures investigated. Additionally, at temperatures above about 1650 K, the decay of propargyl radicals stemming from (R 12) $C_3H_3 \leftrightarrow C_3H_2 + H$ turns out to be essential. This is true for *both* investigated reactants, 1,3-butadiene and 2-butyne (see Figs. 6a and 7 for 1,3-butadiene as reactant, and Figs. 6b and 8 for 2-butyne as reactant, respectively). Furthermore, reaction (R 12) is crucial for describing the level of H-atom production, whereas reaction (R 1) in particular has a remarkable influence on the dynamics of the experimental H-concentration time profiles (see Figs. 7 and 8).

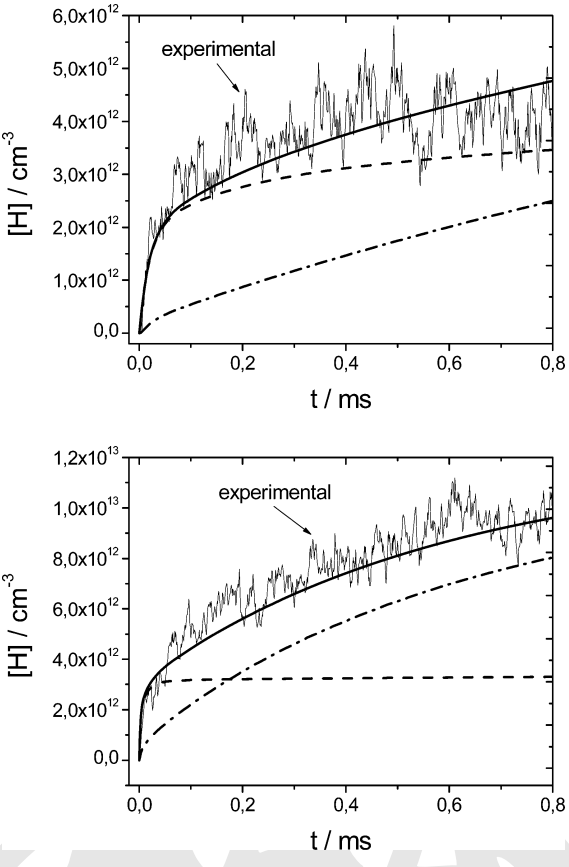

Fig. 8. Influence of reactions (R 1) and (R 12) on H-atom production. Solid curve: full mechanism; dashed curve: without (R 12); dash-dotted curve: without (R 1). Top: T_5 = 1579 K, p_5 = 1.91 bar, $[2\text{-}C_4H_6]_0$ = 3.9 ppm, diluted with argon. Bottom: T_5 = 1770 K, p_5 = 1.92 bar, $[2\text{-}C_4H_6]_0$ = 2.0 ppm, diluted with argon.

3.4.1 Comparing 2-butyne and 1,3-butadiene experiments

Experiments of both types of reactants conducted under similar conditions were analyzed by comparing the ratio of H-atoms produced to the reactants' initial concentration as shown in Fig. 3. For 1,3-butadiene, this ratio is smaller over the whole temperature range covered by the measurements. In the case of 2-butyne as reactant, more H-atoms will be produced at lower temperatures compared to 1,3-butadiene.

If the pyrolysis process started with 2-butyne as reactant, then reaction (R 1) $2\text{-}C_4H_6 \leftrightarrow 2\text{-}C_4H_5 + H$ is the initial reaction step directly producing H-atoms. On the other hand, if the pyrolysis process is started with 1,3-butadiene as reactant, reaction (R 1) is a subsequent reaction occurring only after the 1,3-butadiene

has undergone isomerisation to 1,2-C_4H_6 and 2-butyne according to the reverse reaction (R 5) 1,2-C_4H_6 ↔ 1,3-C_4H_6 and reaction (R 2) 1,2-C_4H_6 ↔2-C_4H_6. The most stable thermodynamic isomer is 1,3-butadiene; hence, the chemical equilibrium of the isomerisation reactions (R 5) 1,2-C_4H_6 ↔ 1,3-C_4H_6 and (R 4) 2-C_4H_6 ↔ 1,3-C_4H_6 is on the right hand side of the reactions. For these reasons, a time delay and a lower level in the formation of H-atoms is observed during the pyrolysis of 1,3-butadiene compared to the pyrolysis of 2-butyne.

3.4.2 Modelling 1,3-butadiene or *2-butyne experiments*

If the 1,3-butadiene experiments have been modelled *separately, without* consideration of the experimental set of 2-butyne, it would be possible to match the H-atom absorption profiles measured during the thermal decay of 1,3-butadiene by the reaction model shown in Table 1, with one exception: for reactions (R 1) 2-C_4H_6 ↔ 2-C_4H_5 + H and (R 2) 1,2-C_4H_6 ↔ 2-C_4H_6, Arrhenius expressions had to be adjusted to those given by Hidaka *et al.* [15]. However, this adjusted reaction model – with the modified Arrhenius parameters for (R 1) and (R 2) – would then predict a much higher rate of H-atom formation if the 2-butyne experiments would be modelled *separately, without* consideration of the experimental set of 1,3-butadiene. Furthermore, a successful description of the 2-butyne experiments with these modified reaction rates for (R 1) and (R 2) would not be possible. Reaction (R 3) 1,3-C_4H_6 ↔ C_2H_4 + C_2H_2 which does not contribute directly to the production of H-atoms below temperatures of 2000 K although it is an important initial reaction step for the thermal decay of 1,3-butadiene.

Now the other way round: Reproducing the 2-butyne experiments by kinetic modelling *separately, without* consideration of the experimental set of 1,3-butadiene, the values for the rate coefficient of reaction (R 1) had to be modified slightly, in order to be consistent with the 1,3-butadiene dataset, although (R 1) is the most important reaction in the 2-butyne system according to the perturbation sensitivity analysis (see Fig. 5b).

Thus, further reactions had to be considered. The isomerisation reaction (R 4) 2-C_4H_6 ↔1,3-C_4H_6 has some influence on the predicted H-concentration profiles for both systems, 1,3-butadiene and 2-butyne. In order to describe the 2-butyne experiments, it would be necessary to adapt the rate coefficient values for (R 4) extensively, by up to a factor of 5, but then it would not be possible to describe *both* experimental datasets, with the *same* reaction model and the *same* set of Arrhenius parameters.

3.4.3 Modelling 1,3-butadiene and *2-butyne experiments*

The perturbation sensitivity plots (Figs. 5a–6b) indicate that the isomerisation reaction (R 2) 2-C_4H_6 ↔ 1,2-C_4H_6 has a much larger influence on the H-atom formation for the 2-butyne system compared to the 1,3-butadiene system. By performing kinetic modelling for reaction (R 2) it was possible to describe *all*

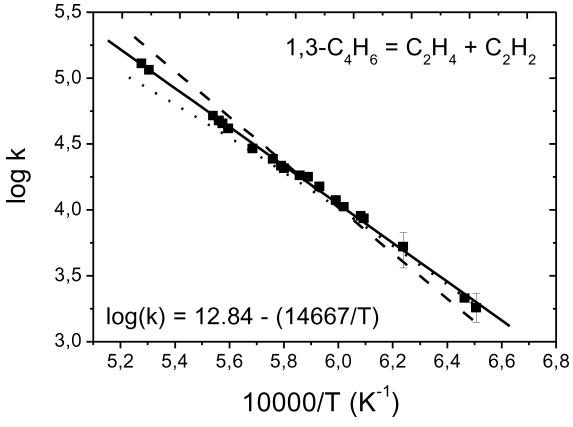

Fig. 9. Arrhenius plot for reaction (R 3): 1,3-C_4H_6 ↔ C_2H_4 + C_2H_2. Symbols & solid curve: present work; dashed curve: Laskin *et al.* [14]; dotted curve: Tsang *et al.* [13].

experimental data. The biggest differences between this work and Hidaka's *et al.* [15] occur for the rate coefficient values for reaction (R 2). Over the investigated temperature range of the experiments carried out in the present work, the values for (R 2) had to be modified by up to a factor of 4. This adaptation was necessary in order to describe *both* the 1,3-butadiene and 2-butyne experiments consistently.

Additionally, the rate coefficient of reaction (R 1) had to be modified slightly compared to the values given in ref. [15].

3.4.4 Importance of reaction (R 3): 1,3-C_4H_6 ↔ C_2H_2 + C_2H_4

The products of the molecular channel (R 3) are ethylene and acetylene. For temperatures below 2000 K, both species are very stable, and do not decompose in notable amounts. Although reaction (R 3) does not contribute directly to the formation of H-atoms, it affects the H-atom profiles indirectly: The faster this reaction channel proceeds, the less the other H-contributing reactions steps will be attended. On the other hand, with respect to the thermal decomposition of 2-butyne, reaction (R 3) has only a minor influence on H-atom formation.

For the reproduction of the 1,3-butadiene *and* the 2-butyne experiments, kinetic modelling of the molecular channel (R 3) was performed. The values of the rate coefficient obtained for reaction (R 3) are plotted in Fig. 9 (solid curve) as a function of temperature. For comparison, Arrhenius expressions published in literature are shown as well and are plotted within the investigated temperature range (dotted curve: Tsang *et al.* [13]; dashed curve: Laskin *et al.* [14]).

The Arrhenius expression obtained by Tsang *et al.* [13] as a result of a master equation analysis is given by $k\,(T)/\,s^{-1} = 4.2 \cdot 10^{88} \cdot T^{-20.85} \cdot \exp(132873\ [cal \cdot mol^{-1}]/RT)$. At temperatures between 1500 and 1900 K, the determined

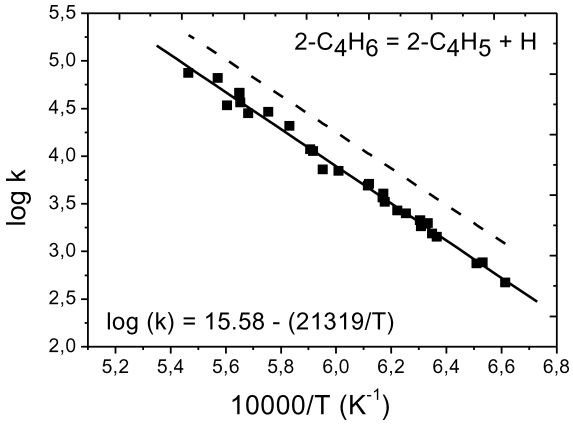

Fig. 10. Arrhenius plot for reaction (R 1): 2-C_4H_6 ↔ 2-C_4H_5 + H. Solid curve, symbols: present work; dashed curve: Hidaka *et al.* [15].

rate coefficient values of the present work are in good compliance. Also, again, good agreement is found between the rate coefficient values obtained in the present work and those reported by Laskin *et al.* [14] for 1,3-butadiene pyrolysis experiments performed between 1100 and 1200 K and reactant concentrations of 3000 ppm, when extrapolating their rate coefficients to the temperature range of the present work.

3.4.5 Importance of reaction (R 1): 2-C_4H_6 ↔ 2-C_4H_5 + H

In principle, we could have also tried to describe the 1,3-butadiene pyrolysis experiments by modelling reaction (R 1). However, if the Arrhenius equation of reaction (R 1) would have been strongly modified as it would have been necessary considering the 1,3-butadiene experiments *alone,* then we would not have been able to reproduce the H-atom profiles measured during the thermal decomposition of 2-butyne. Additionally, it should be mentioned that the Arrhenius equation for the decomposition of propargyl radicals according to (R 12) that turned out to have an important impact on the amount of H-concentration profiles (see e.g. Fig. 8) was not changed at all, as this reaction was investigated in an experimental H-ARAS shock tube study by Scherer [32] under conditions comparable to the present experiments.

All derived values of the rate coefficient of reaction (R 1) are plotted in Fig. 10 (symbols, solid curve), as a function of temperature. For comparison, the Arrhenius expression published by Hidaka *et al*. [15] resulting from quantum RRKM calculations is given as well for the temperature range covered by the experiments of the present work.

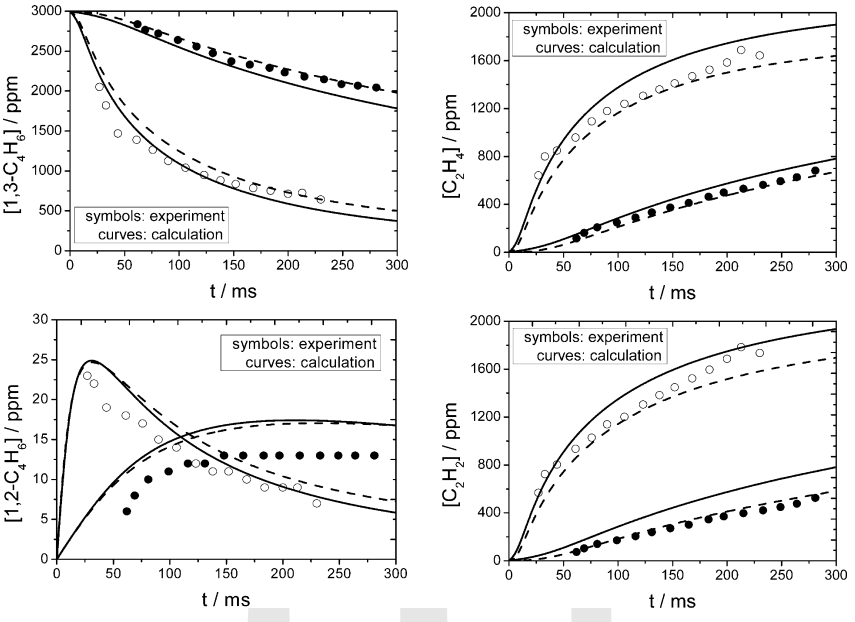

Fig. 11. Experimental (symbols, Laskin *et al.* [14]) and computed (curves) concentration profiles during the pyrolysis of 3000 ppm 1,3-butadiene diluted with nitrogen; p = 1 atm; T = 1110 K (open circles) and T = 1185 K (full circle). Dashed curve: calculations with reaction model and Arrhenius parameters given by Laskin *et al.* [14]; solid curve: reaction model by Laskin *et al.,* but Arrhenius parameters from present work.

3.4.6 Check of the elaborated reaction model

As a check of the reaction model derived in the present work from modelling H-atom profiles obtained during the thermal decay of 1,3-butadiene and 2-butyne, respectively, further simulations were performed using pyrolysis experiments reported by Laskin *et al.* [14] for temperatures between 1100 and 1200 K and reactant concentrations of 3000 ppm 1,3-butadiene.

A comparison of calculated and measured concentration profiles of 1,3-butadiene and some major product components such as 1,2-C_4H_6, C_2H_4, and C_2H_2, are shown in Fig. 11. For these calculations, the same reaction model given by Laskin *et al.* [14] was used with the same rate coefficients (Fig. 11, solid curve). If the rate coefficients derived from the present work were used, minor differences in the calculated species profiles were obtained. Overall, very good agreement was found despite the different temperature regimes of the two experimental studies.

4. Conclusions

The thermal decomposition of two different reactants, 1,3-butadiene (1,3-C_4H_6) and 2-butyne (2-C_4H_6), respectively, were investigated in a high purity shock tube device over a temperature range of about 1500–1800 K at total pressures between 1.2 and 1.9 bar, highly diluted with argon. The formation of H-atoms was measured as a function of time behind reflected shock waves by using the very sensitive method of atomic resonance absorption spectrometry (ARAS). With help of sensitivity and reaction flux analysis and by modelling *both* sets of experimental data *simultaneously*, a detailed chemical kinetic reaction mechanism was generated. This reaction model which comprises 33 elementary reactions and 26 species was proven to match the experimentally obtained H-atom profiles.

Acknowledgement

The authors like to thank N. Ackermann for his help with the analysis procedure. Furthermore, S.P. is thankful for funding within the Collaborative Research Centre 606 "Non-stationary Combustion: Transport Phenomena, Chemical Reactions, Technical Systems".

References

1. P. Dagaut, Phys. Chem. Chem. Phys. **4** (2002) 2079–2094.
2. A. J. Dean, O. G. Penyazkov, K. L. Sevruk, and B. Varatharajan, Proc. Comb. Inst. **30** (2007) 2481–2488.
3. U. Steil, M. Braun-Unkhoff, P. Frank, M. Aigner, Paper No. 973, 46th AIAA Aerospace Sciences Meeting and Exhibit 7–10 Jan 2008, Reno, Nevada (USA).
4. N. Slavinskaya, Paper No. 0992, 46th AIAA Aerospace Sciences Meeting and Exhibit 7–10 Jan 2008, Reno, Nevada (USA).
5. C. Wahl, M. Kapernaum, EU-project CFD4C, final report, project no. GRDl-1999–10325 (2001).
6. G. Dayma, G. R. Fournet, F. Battin-LeClerc, Int. J. Chem, Kinet. **35** (2003) 273.
7. U. Steil, M. Braun-Unkhoff, C. Naumann, P. Frank, European Combustion Meeting, Louvain la Neuve, Belgium (2005).
8. G. B. Skinner, E. M. Sokolowski, J. Phys. Chem. **64** (1960) 1028.
9. S. W. Benson, G. R. Haugen, J. Phys. Chem. **71** (1967) 1735.
10. J. H. Kiefer, H. C. Wei, R. D. Kern, C. H. Wu, Int. J. Chem. Kinet. **17** (1985) 225.
11. J. H. Kiefer, K. I. Mitchell, H. C. Wei, Int. J. Chem. Kinet. **20** (1988) 787.
12. V. S. Rao, K. Takeda, G. B. Skinner, Int. J. Chem. Kinet. **20** (1988) 153.
13. W. Tsang, V. Mokrushin, Proc. Combust. Institute **28** (2000) 1717.
14. A. Laskin, H. Wang, C. K. Law, Int. J. Chem. Kinet. **32** (2000) 589.
15. Y. Hidaka, T. Higashihara, N. Ninomiya, H. Masaoka, T. Nakamura, H. Kawano, Int. J. Chem. Kinet. **28** (1996) 137.
16. Y. Hidaka, T. Higashihara, N. Ninomiya, H. Oshita , H. Kawano, J. Phys. Chem. **97** (1993) 10977.
17. Y. Hidaka, T. Higashihara, N. Ninomiya, T. Oki, H. Kawano, Int. J. Chem. Kinet. **27** (1995) 331.

18. S. D. Chambreau, J. Lemieux, L. Wang, J. Zhang, J. Phys. Chem. A **109** (2005) 2190.
19. C. Xu, M. Braun-Unkhoff, C. Naumann, P. Frank, Proc. Combust. Inst. **31** (2007) pp. 231–239.
20. J. K. Wright, *Shock Tubes*. Methuen & Co Ltd, Great Britain (1961).
21. W. Tsang, A. Lifshitz, Ann. Rev. Phys. Chem. **41** (1990) 559.
22. Th. Just in *Shock waves in chemistry*. A. Lifshitz (Ed.), M. Dekker, New York (1981) 279.
23. D. A. Masten, R. K. Hanson, C. T. Bowman, J. Phys. Chem. **94** (1990) 7119.
24. P. Frank, Th. Just, Ber. Bunsenges. Phys. Chem. **89** (1985) 181.
25. A. E. Lutz, R. J. Kee, J. A. Miller, SENKIN: A fortran program for predicting homogeneous gas phase chemical kinetics with sensitivity analysis, Sandia National Laboratories, Livermore, CA 94551–0969, report SAND87–8248, February (1988).
26. H. Wang, University of California at Los Angeles (USA) 2000. http://ignis.usc.edu/Mechanisms/C4H6/c4h6.html
27. A. Burcat Technion Institute Haifa, Israel (2007), ftp://ftp.technion.ac.il/pub/supported/aetdd/thermodynamics,
28. S. W. Benson, *Thermochemical Kinetics*. John Wiley & Sons, USA (1976).
29. H. Wang, M. Frenklach, Combust. Flame **110** (1997) 173.
30. V. D. Knyazev, I. R. Slagle, J. Phys. Chem. **100** (1996) 16899.
31. K. M. Leung, R. P. Linstedt, Combust. Flame **102** (1995) 129.
32. S. Scherer, Ph. D. Thesis, University of Stuttgart (2001).
33. N. Belmekki, P. A. Glaude, I. Da Costa, R. Fournet and F. Battin-Leclerc, Int. J. Chem. Kinet. **34** (2002) 172.
34. D. L. Baulch, C. J. Cobos, R. A. Cox, P. Frank, G. Hayman, Th. Just, J. A. Kerr, T. Murrells, M. J. Pilling, J. Troe, R. W. Walker, J. Warnatz, J. Phys. Chem. Ref. Data **23** (1994) 847.
35. V. Venkatesh, R. K. Hanson, D. M. Golden, C. T. Bowman, D. F. Davidson, J. Phys. Chem. A **111** (2007) 4062.
36. D. L. Baulch, C. J. Cobos, R. A. Cox, C. Esser, P. Frank, Th. Just, J. A. Kerr, M. J. Pilling, J. Troe, R. W. Walker, J. Warnatz, J. Phys. Chem. Ref. Data **21** (1992) 411.
37. M. Braun-Unkhoff, A. Kurz, P. Frank, Proceedings of the 17th International Symposium on Shock Waves (1989) 493.
38. H. Wang, Ph. D thesis, The Pennsylvania State University, University Park, PA, USA (1992).